Fabrication and characterization of nanostructured immiscible Cu-Ta alloys processed by high-pressure torsion

Tayebeh Mousavi[1], Jiaoyan Dai[2,*], Piotr Bazarnik[3], Pedro Henrique R. Pereira[4],

Yi Huang[5,6,*], Malgorzata Lewandowska[3], Terence G. Langdon[6]

[1]Materials Department, University of Oxford, Oxford OX1 3PH, UK

[2]School of Materials and Chemical Engineering, Ningbo University of Technology, Ningbo 315211, P.R. China

[3]Faculty of Materials Science and Engineering, Warsaw University of Technology, Woloska 141, 02-507 Warsaw, Poland

[4]Department of Metallurgical and Materials Engineering, Universidade Federal de Minas Gerais, Belo Horizonte, MG 31270-901, Brazil

[5]Department of Design and Engineering, Faculty of Science and Technology, Bournemouth University, Poole, Dorset BH12 5BB, UK

[6]Materials Research Group, Department of Mechanical Engineering, University of Southampton, Southampton SO17 1BJ, UK

Abstract

Nanostructured Cu–Ta alloys show great potential as high strength nanocrystalline materials due to their excellent mechanical properties and limited grain growth at high temperatures. This report describes the fabrication of nanostructured immiscible Cu-Ta alloys in bulk by high-pressure torsion (HPT) using a stack of Cu/Ta/Cu discs at room temperature. A microstructural study after HPT processing showed that the internal Ta layer breaks into small individual flakes which distribute uniformly over the Cu matrix through increases in the numbers of HPT turns. There is solid-state diffusion between the Cu and Ta when the HPT processing increases to 100 turns due to microstructural refinement and increasing crystalline defects. After processing through 150 turns, a composite microstructure of two phases is formed including supersaturated Cu-Ta solid solutions ($Cu_{81}Ta_{19}$ and $Ta_{78}Cu_{22}$ alloys) with a crystallite size of ~35-45 nm. This fine microstructure produces exceptional mechanical properties including a high hardness of over 350 Hv corresponding to ~3.43 GPa, a tensile strength of ~1300 MPa and a tensile elongation of about 40%.

Keywords: Cu-Ta alloys; high-pressure torsion; nanostructures; severe plastic deformation.

*Corresponding authors: Jiaoyan Dai (jydai@nbut.edu.cn), Yi Huang (yhuang2@bournemouth.ac.uk)

1. Introduction

Nanostructured alloys have attracted significant interest due to their unique sets of properties which are not achievable in coarse-grained polycrystalline materials [1,2]. Non-equilibrium solid solutions have also drawn attention as they can evolve as nanoscale microstructures through processing and then form well-dispersed nanoscale composites upon annealing at elevated temperatures [3]. Both simulations and experiments indicate remarkable physical and mechanical properties for this new class of material. The Cu-Ta system is one of these immiscible systems with almost zero solubility of Cu(Ta) in Ta(Cu) at room temperature (RT) [4].

Several processing methods are available for producing nanocrystalline microstructures consisting of solid solutions having different elements. For example, processing through the introduction of severe plastic deformation (SPD) has been used successfully over the last two decades to generate non-equilibrium microstructures in a range of metals and alloys [5-7]. Potential SPD techniques, including equal-channel angular pressing (ECAP) [8,9], accumulative roll bonding (ARB) [10] and high-pressure torsion (HPT) [11-13], have the potential of not only producing nanocrystalline microstructures but also of generating alloys of immiscible systems due to the extra crystalline defects and dislocations that are introduced into the matrix through the SPD processing. This excess of defects will thereby facilitate diffusion in these systems leading to the production of non-equilibrium solid solutions.

In general, the HPT process is usually considered the most effective procedure for achieving exceptional grain refinement, typically to the nanometer range in many systems, and this has become an established processing method for studying nanocrystalline and non-equilibrium solid solutions. In HPT processing, grain refinement may be achieved without cracking due to the imposed hydrostatic pressure which effectively prevents the propagation of fracture during the torsional straining [14]. Recently, FEM modelling [15-18] and experimental

observations on two phase materials such as duplex stainless steel [19-24] and Cu-Ag alloys [25] demonstrated that, in addition to the in-plane shear strain, there is also mass transfer within the samples in HPT due to the development of turbulent eddy flows within the sample cross-sections during the processing [26]. It is evident that this will assist in the redistribution of metal components in an immiscible system.

The synthesis of novel nanostructured alloys formed from forced solid solutions, especially for the non-equilibrium solid solutions such as Cu and immiscible solute species, has been the focus of some recent studies [27,28]. For example, mechanical alloying has been used to generate Cu-based powders composed of immiscible alloying elements such as Ta [29] and Mo [30] where these systems have shown moderate to extraordinary high microstructural stability at elevated temperatures. There are also recent reports on the thermal stability and microstructure of high strength nanocrystalline Cu–Ta alloys [29]. For example, isothermal annealing of a Cu–10% Ta powder produced via high-energy cryogenic mechanical alloying led to a nanocrystalline, two-phase composite structure of spheroidal Ta particles and nanolamellar Ta dispersed in a Cu-rich Cu–2% Ta alloyed matrix [29]. It is important to note also that the consolidation of nanostructured powder into a bulk form is often very challenging because of limitations associated with the processing methods that are not easily scalable or due to uncontrolled grain growth of the non-equilibrium structures during processing. Despite the excellent properties achieved in these Cu-Ta alloys via mechanical alloying, there is only a limited report on the fabrication of nanostructure Cu-Ta alloys through processing a mixture of bulk Cu and bulk Ta, where the initial disc samples were a $Cu_{50}Ta_{50}$ system consisting of 19 Cu foils and 18 Ta foils assembled alternately in a single stack and successfully processed by HPT to 10, 30, 50, 100 and 150 turns under a pressure of 4.0 GPa [31]. It is noted that the HPT-processed 150 turns Cu-Ta alloy showed a superior thermal stability even after annealing at 1000°C for 1h [31].

The HPT processing of the $Cu_{50}Ta_{50}$ system [31] has limitations in its practical fabrication due to the difficulty and time required to prepare Cu foils and Ta foils, where the foil thickness is only ~24.3 µm, in order to make the 0.9 mm thick disc sample of stacked 19 Cu foils and 18 Ta foils before HPT processing. To improve the efficiency in materials preparation and processing, the present research was initiated to process immiscible Cu-Ta alloys using bulk Cu discs and Ta discs (thickness 0.8 mm for each Cu disc and Ta disc) which were packed in a sandwich-like structure of Cu/Ta/Cu for HPT processing. The microstructures and mechanical properties of the HPT-processed Cu-Ta alloys were subsequently investigated in detail. As will be demonstrated, the use of HPT processing produces a material having exceptionally high hardness and excellent tensile strength.

2. Experimental materials and procedures

The experiments were conducted using rods of oxygen-free Cu (99.95 wt.%) and Ta (99.9 wt.%). The Cu rod was first annealed for 1 h at 673 K whereas the Ta rod was received in an annealed state. Both the annealed Cu rod and the as-received Ta rod were cut into discs with diameters of 10 mm and thicknesses of 1.1 mm and this was followed by grinding to a thickness of 0.8 mm. Then a Ta disc was placed between two Cu discs in a sandwich-like configuration and the piled discs were processed by HPT at room temperature through total numbers of turns, *N*, of 0.25, 5, 10, 60, 100 and up to a maximum of 150 turns. The HPT processing was conducted using an applied pressure of 6.0 GPa and a rotation speed of 1 rpm under quasi-constrained conditions where there is a small outflow of material around the edge of the disc between the two anvils [32].

Various characterization techniques and hardness measurements were carried out on the processed discs in order to provide information on the microstructural evolution and mechanical properties achieved through the HPT processing.

The X-ray diffraction (XRD) was performed on a Rigaku SmartLab employing Cu Kα radiation (wavelength λ = 0.154 nm) at 45 kV and a tube current of 200 mA. The XRD measurements covered an angular 2θ range from 30° to 130° using a scanning step of 0.04° and a scanning speed of 2° min^{-1}. Microstructural characterization was conducted on the cross-sections of the discs using analytical scanning electron microscopy (SEM). A JEOL 5510 SEM with OI SDD detector operating at 20 kV accelerating voltage and an Hitachi SU-8000 SEM operating at 10 kV were used for microstructural examinations. The specimens were prepared by cutting the processed disc into halves along the dimeter and polishing the cross-sections using an Hitachi Ion Milling System IM-4000. Since ion milling is a damageless process, this polishing eliminates all deformation and oxide layers so that the surface quality was sufficiently good for SEM analysis. High resolution microstructural analysis was carried out using a transmission electron microscope (TEM, JEOL3000F) on cross-sectional samples made by the lift-out technique in focused ion beam (FIB) milling. The polished surface of the 150 turns sample was also observed using a scanning transmission electron microscope (STEM, Hitachi HD-2700) in both bright-field (BF) and high-angle annular dark field (HAADF or Z-contrast) modes to reveal the grain structures at higher magnifications.

Measurements of the Vickers microhardness, Hv, were carried out using an FM300 microhardness tester equipped with a Vickers indenter. For these measurements, the HPT-processed discs were carefully ground with SiC papers in order to remove layers of 0.1 mm thickness from the disc surfaces. The discs were then polished with 9, 6, 3 and 1 μm diamond suspensions and polished to a mirror-like surface with 0.04 μm colloidal silica. Each hardness indentation was performed using a load of 200 gf and a dwell time of 15 s. Separate measurements were carried out at points along the disc diameter from the bottom to the top of the cross-section. The minimum distance between consecutive indentations was 150 μm in order to avoid any interference between the individual measurements. Colour-

coded contour maps were constructed in which the individual hardness values were displayed using a colour scale and these values were plotted as a function of location on the cross-sections of the discs.

Tensile specimens were cut from the HPT-processed 150 turns samples. Following earlier practice [33], two tensile specimens were prepared from each disc using electro-discharge machining with these specimens arranged symmetrically on either side of the disc centre. The miniature tensile specimens had gauge lengths and widths of 1 mm. These specimens were then tested in tension at room temperature using a Zwick 30 KN Proline testing machine operating at a constant rate of cross-head displacement with an initial strain rate of 1.0×10^{-3} s^{-1}. The elongations were calculated by measuring the gauge length after tensile testing by putting the two parts of the broken tensile specimen together under an optical microscope. Three tests were repeated for each tensile curve.

3. Experimental results

3.1 Initial microstructural characteristics after HPT processing

The cross-sections of the HPT-processed samples were first observed using an optical microscope (OM) to examine the evolution of the stacked Cu-Ta-Cu layers. As shown in Fig. 1, after 0.25 HPT turn the bulk Ta layer is clearly visible between the two Cu bulk layers and there are sharp and distinct Cu-Ta interfaces. After 5 and 10 turns of HPT processing, in some areas the Cu-Ta boundaries disappear but in some regions the Cu-Ta interfaces are distinct but with significant curvature. When the HPT processing increases to 60 and 100 turns, the Cu and Ta appear to mix well in the disc edge area where there is a grey background colour which lies between the dark Ta and bright Cu and at the edge there are also no obvious Cu-Ta boundaries at the magnification used for the OM. However, in the central area after 60 and 100 HPT turns there is evidence for thin and fine Cu-Ta interfaces. After 150 turns of HPT processing, no obvious Cu-Ta boundaries are observed at any position in the OM, thereby indicating a fully-

homogeneous mixing of Cu and Ta. Based on these observations from Fig. 1, it is concluded that, by increasing the numbers of HPT turns, there is a gradual increase in homogeneity as a result of mixing of the Cu and Ta and this homogeneity occurs initially in the edge regions but gradually expands to fill the disc with increasing numbers of HPT turns.

In order to evaluate the homogeneity of the 150 turns sample at a finer scale, the cross-section of the sample was observed by SEM at different positions within the central area and the edge area of the disc: Examples are shown in Fig. 2(a) and (b) where the upper image depicts the cross-section after 150 turns and marks the two positions for the subsequent SEM images. It is apparent from these images that both areas show a layered microstructure which is slightly finer within the region close to the edge. Thus, in the central region the layers are almost straight whereas in the edge region the layers are curved. This is attributed to the strain gradient imposed in the HPT processing since higher strains are attained at the edge than in the central region. Elemental maps of Cu and Ta are presented at higher magnifications in Fig. 2(c-f) for the small regions marked by squares in Fig. 2(a) and (b). As can be seen, the layered microstructure includes Cu-rich regions and Ta-rich regions at the fine scale. Furthermore, the Cu-rich regions contain Ta and similarly the Ta-rich regions contain Cu, thereby demonstrating that the Cu and Ta have dissolved into each other. The EDX line-scans across these layers shown in Fig. 2(g-h) indicate that the Cu layers contain about 18-21 at.% Ta and the Ta layers contain about 19-23 at.% Cu. Also, the Cu-rich and Ta-rich layers are within a few micrometers in both the central and edge regions. Thus, HPT processing through 150 turns leads to a fine layered microstructure and this structure uniformly covers the whole sample. It is important to note that in this condition there is no detectable pure Cu or pure Ta remaining in the microstructure and instead the immiscible Cu and Ta are visibly mixed to create Cu-Ta alloys through the HPT processing.

3.2 Data from X-ray diffraction

The XRD patterns of the Cu-Ta samples processed by HPT through different numbers of turns (0.25, 5, 10, 60, 100 and 150) are shown in Fig. 3. Inspection shows that there is a systematic decrease in the relative intensities of the Cu and Ta peaks as well as a broadening of the peaks with increasing numbers of turns. The broadening of the Cu and Ta peaks is due to the effect of refinement in the crystallite size and the concomitant increase in internal strain.

The crystallite sizes and lattice distortions of the Cu and Ta were determined using the Williamson–Hall equation [34] and the results are presented in Fig. 4 as a function of the number of HPT turns: the instrumental broadening was considered in this analysis by using Si as a standard sample. Thus, the crystallite sizes of Cu and Ta decrease to less than 150 nm after 60 turns and further refinement occurs gradually up to 150 turns with final values of ~35 and ~45 nm for Cu and Ta, respectively. The lattice microstrain increases to high values of about 1.8% and 1.4% after 150 turns for Cu and Ta, respectively. Such crystallite size refinement to the nanoscale and high lattice strain accumulates within the sample as a result of the high pressure and high shear strains imposed in HPT processing. Similar reductions in grain size were reported in other systems [11,12] and they confirm the potential for using HPT to achieve grain sizes in the nanometer range.

After 100 and 150 turns in Fig. 3, the XRD data show that the Ta diffraction peaks are shifted towards higher angles and the Cu diffraction peaks are shifted towards lower angles through increasing numbers of turns. This confirms changes in the lattice parameters of Ta and Cu above about 100 turns due to the mutual dissolution of Cu and Ta. The atomic radius of Ta is larger than Cu and therefore, as a result, the Ta crystal lattice is reduced in size when Cu atoms replace some of the Ta atoms thereby causing a peak shift towards higher angles. Similarly, the Cu crystal lattice increases in size and the Cu peaks shift to lower angles due to

the dissolution of the larger Ta atoms in the Cu lattice. This indicates that Cu-Ta alloys are formed by the HPT process and this is consistent with the SEM images in Fig. 2.

A further analysis of the XRD data by Materials Analysis Using Diffraction (MAUD) [35] to compute the mean lattice parameter of the metastable Cu-Ta alloy and Vegard's law [36] gave an average concentration of Cu in Ta as ~21.0 at.% and an average concentration of Ta in Cu estimated as ~18.5 at.% throughout the entire disc. It is noted that, consistent with the EDX data, these values are remarkably high when using a processing route involving a bulk-state reaction without the application of an elevated processing temperature.

3.3 Results from TEM and STEM observations

Fig. 5 shows high magnification TEM images of different cross-sectional positions for the disc processed through 150 turns where the images (a) to (c) relate to the positions shown on the upper bulk sample. In these images, the Ta-rich regions are in dark colour and it is apparent that the microstructures in all regions consist of a matrix of Cu-rich Cu-Ta alloy with a secondary Ta-rich region distributed throughout the matrix. Comparing Figs 5 (a-c), it appears that the microstructure closer to the edge is more uniform. In practice, the Ta-rich regions are well distributed over the matrix but their size and shape are different at the centre and edge of the disc. At the centre the Ta-rich regions are relatively coarse and have a layered shape ~20-200 nm in width and ~0.1-1.0 μm in length whereas at the edge these regions are individual flakes with a much finer size. It can be seen also that the Ta-rich regions with layered shapes present throughout the disc centre, as well as the flakes at the edge, lie essentially perpendicular to the direction of the anvils.

High magnification images from the matrix in the edge region, given in Figs 5 (d,e), show that the Cu-rich matrix contains very fine grains as well as Ta-rich clusters on a very fine scale of the order of ~5-10 nm. An atomic resolution TEM image of the interface between these nano-scale Ta-rich clusters and the Cu-rich matrix, shown in Fig. 5(f), reveals a strong atomic

bonding with no evidence for any porosity and/or cracks as a result of any enhanced diffusion occurring between the Cu and Ta through the HPT processing. The *d*-spacing extracted from the high resolution TEM image shows *d*-spacing values of ~0.142 nm and ~0.205 nm for the Cu-rich matrix and the Ta-rich region, respectively, where these values correspond to (022) for Cu and (011) for Ta. Comparing these values with the theoretical values, given by d_{022} (Cu) = 0.128 nm and d_{011} (Ta) = 0.233 nm [37], it is apparent that there is a small expansion in the Cu lattice and a slight contraction in the Ta lattice due to the dissolution of large Ta atoms in Cu and small Cu atoms in Ta.

Fig. 6(a) shows an STEM image of the 150 turns disc in the half-radius area, corresponding to ~3 mm from the disc centre area, with the Ta-rich regions appearing black, and Fig. 6(b) is an HAADF image (or a Z-contrast image) of the same area. In Z-contrast images the heavy elements are bright and therefore the Ta-rich regions are now brighter. Thus, again the Ta-rich regions show good bonding with the Cu matrix with no detection of any cracks or voids after processing to 150 turns and with a size for the Ta-rich regions in the range of ~5-40 nm. These conclusions are therefore consistent with the TEM data shown in Fig. 5.

3.4 Hardness and mechanical properties of the Cu-Ta alloy after HPT processing

Fig 7 shows colour-coded contour maps depicting the hardness values throughout cross-sections of the discs after HPT processing through different numbers of turns (0.25, 10, 100 and 150 turns). With reference to the scale for the values of Hv shown on the right, it can be seen that the microhardness increases significantly with increasing numbers of turns. Before HPT processing the annealed Cu and the as-received Ta showed average Vickers microhardness values of ~41 and ~200 Hv, respectively. After 0.25 turn the hardness was similar to the pure Cu and pure Ta but after 10 turns the hardness in the regions close to the edge of the disc increased to ~300 Hv whereas the hardness in the central section of the disc remained almost unchanged.

Further HPT deformation up to 100 turns gave an additional increase to nearly ~350 Hv across the discs except for a few small areas near the centre of the discs and an overall saturation hardness of ~350 Hv was achieved over the entire disc after 150 turns. The increase in microhardness from the centre to the edge is due to the low strain imparted in the central region during HPT processing and this trend matches results reported for many other metal systems [38, 39]. Thus, after 150 turns the microhardness is reasonably homogeneous throughout the disc with an average value of ~350 Hv which is equivalent to a hardness of ~3.43 GPa. This hardness is very much higher than the initial hardness values of the pure Cu and pure Ta and the results demonstrate the remarkable hardness increases that may be achieved by processing through HPT.

Fig. 8 shows a stress-strain curve for the 150 turns sample tested at RT using an initial strain rate of 1.0×10^{-3} s^{-1}. Thus, the Cu-Ta alloy processed by HPT for 150 turns exhibits an ultimate tensile strength (UTS) of ~1300 MPa and a tensile elongation of about 40%. This very high strength is due to the microstructure achieved by the HPT processing and it is important to note that the UTS in this experiment is very much higher than the conventional values anticipated for pure copper (~150-300 MPa) and pure tantalum (~180-220 MPa) [40]). The HPT-processed Cu-Ta alloy also exhibits an acceptable elongation close to ~40%.

4. Discussion

An evaluation of the microstructure and the phase evolution of the Cu-Ta sample through the HPT processing shows that in the early stages the Ta layer within the stack becomes thinner as a result of the HPT shear strain and then gradually these thin Ta layers are broken to form small flakes. The size of these Ta-rich flakes decreases as the HPT process continues and ultimately there is essentially a uniform dispersion of flakes throughout the Cu matrix. Since the edge area of the disc experiences a higher strain than the central region, the microstructural evolution occurs initially from the edge and then gradually extends to the centre with increasing

numbers of HPT turns. As a result, the microstructure at the edge becomes more homogenous with smaller Ta-rich regions in the early stages but, by increasing the numbers of turns, most of the disc develops into a reasonably homogenous Cu-Ta alloy as a result of the accumulated strains operating through the whole disc.

This microstructural evolution is illustrated schematically in Fig. 9 where the microstructure evolves from left to right to ultimately produce a bulk Cu-Ta alloy. The microstructural features demonstrated in Fig. 9 are consistent with a Cu-Ta alloy processed by HPT from a disc with a stack of 19 Cu foils and 18 Ta foils [31] where the microstructure was a mixture of ultrafine grains corresponding to a Cu-16% Ta solid solution with embedded nano-scaled Ta-rich particles. Thus, the strategy in this research of using a disc sample with a pack of sandwich-like Cu/Ta/Cu discs for HPT processing was very effective in producing a bulk nanostructured immiscible Cu-Ta alloy. Computer modelling has confirmed the occurrence of turbulent flow in the cross-sections of HPT samples [15, 16] and this may assist in the mass transfer and redistribution of metal components in the immiscible Cu-Ta system.

By increasing the numbers of HPT turns to give increased strain, there is additional grain refinement in the matrix and there are more crystalline defects thereby creating new diffusion paths for the Cu and Ta atoms. According to the XRD data, excess diffusion occurs after about 100 HPT turns. The crystallite sizes of Cu and Ta after 100 turns are ~95 and ~64 nm, respectively, and this corresponds to size reductions of ~66% and ~70 % for Cu and Ta, respectively. Such large reductions in crystallite size could increase the fractions of grain boundaries which are known as effective diffusion path in this system [41]. It is therefore concluded that, after about 100 HPT turns, the numbers of grain boundaries and crystalline defects are sufficiently high to create practical diffusion paths for the Cu and Ta atoms.

In addition to the large numbers of grain boundaries and crystalline defects, the Ta-rich layers become finer with increasing HPT turns and this will also contribute to diffusion of Cu

and Ta leading to the production of solid solutions in the immiscible Cu-Ta system. According to the present XRD and EDX data, after 150 HPT turns the concentration of Cu in Ta is about 22% and the concentration of Ta in Cu is about 19% generating the $Ta_{78}Cu_{22}$ and $Cu_{81}Ta_{19}$ alloys. These solubility values are remarkably high for the immiscible Cu-Ta system when it is noted that Cu and Ta have different crystalline structures (face-centred cubic and body-centred cubic, respectively) and negligible mutual solubility in the solid state [4]. It is especially notable also that such high solubility has been achieved in this investigation using a processing route which involves a bulk-state reaction at RT without the necessity of applying an elevated processing temperature. This indicates that the HPT process is capable of forcing a significant amount of Ta into a metastable FCC solid solution with Cu at room temperature.

The results show also that the final microstructure after 150 HPT turns is a composite containing a Cu-rich matrix with a crystallite size of ~45 nm and fine Ta-rich layers with a size of about 100-500 nm and a crystallite size of ~35 nm which is dispersed evenly within the matrix. In addition to these Ta-rich layers, Ta-rich clusters are also present and they are reasonably uniformly distributed in the microstructure but on a much finer scale of <10 nm. Such a microstructure achieved by HPT processing leads to very significant improvements in the mechanical properties.

A high UTS of ~1300 MPa with an acceptable elongation of about 40% was measured for the sample subjected to 150 turns. Measurements showed that the microhardness value was almost uniform throughout the whole disc after 150 turns with an average value of ~350 Hv which is equivalent to ~3.43 GPa. A comparison of this microhardness value with pure nanocrystalline Cu of similar grain size shows a strength increase by more than a factor of three. Thus, the hardness was reported as ~102 Hv for pure Cu with a grain size of ~35 nm [42] and this may be compared with the present hardness of ~350 Hv for the HPT-processed Cu–Ta alloy having the same grain size of ~35 nm. The final hardness value achieved in this

investigation after 150 turns is also almost two times higher than the value reported for Cu-Ta alloys fabricated by magnetron sputtering [43].

Although the HPT-processed 150 turns Cu-Ta alloy has a much higher UTS (~1300 MPa) than pure Cu (~150-300 MPa) and pure tantalum (~180-220 MPa) [40] fabricated by conventional thermomechanical processing methods, it is of interest to compare the strength of HPT-processed Cu-Ta alloy with that of HPT-processed pure Cu and pure Ta. The strength of HPT-processed pure Ta and pure Cu are ~1300 MPa [44] and ~460 MPa [45] respectively. This means that the strength of the HPT-processed Cu-Ta is very close to that of the HPT-processed pure Ta. Considering the Cu-Ta alloy developed initially from Cu/Ta/Cu packed discs, the developed immiscible Cu-Ta alloy has a greater Cu component than Ta component but the minor component Ta appears to make a larger contribution to the strength of the HPT-processed Cu-Ta alloy.

In order to understand the strengthening mechanism of the HPT-processed immiscible Cu-Ta alloy, it is necessary to analyse the relationship between the microstructure and mechanical properties. As shown in Fig. 5, the microstructure of the HPT-processed Cu-Ta alloy contains Ta-rich clusters on a very fine scale of the order ~5-10 nm within the Cu-rich matrix where the Cu-rich matrix consists of a matrix of a Cu-rich Cu-Ta alloy with secondary Ta-rich flakes distributed throughout the matrix. This means that the dominant Cu-rich layers and sparsely distributed Ta-rich flakes form the matrix of the Cu-Ta alloys.

Elemental mapping by SEM in Fig. 2 and x-ray analysis in Fig. 3 confirm that a Cu-Ta solid solution formed in the Cu-rich layers and Ta-Cu solid solutions formed in the Ta-rich flakes, and significant grain refinement was achieved in both the Cu-rich and Ta-rich regions. Based on microstructural analysis, the high strength of the HPT-processed immiscible Cu-Ta alloy is attributed to a combination of several strengthening mechanisms. Thus, solid solution strengthening exists in both the Cu-rich layers and Ta-rich flakes and this will make a

contributions to the overall strength. In addition, the interfaces between the Cu-rich layers and the Ta-rich flakes in the matrix will provide an extra barrier to dislocation movement in addition to the grain boundaries, and the significant grain refinement due to the heavy shear strain applied during the HPT processing will also enhance the material strength. Finally, the nanoscale Ta-rich clusters will act as a dispersed hard phase in the Cu-rich matrix giving a dispersion strengthening effect.

The elongation of ~40% obtained in the 150 turns HPT-processed immiscible Cu-Ta alloy demonstrates that this new Cu-Ta alloy exhibits a good balance between high strength and reasonable ductility. Normally, the material strength and ductility are incompatible so that high strength leads to a reduced ductility. The tensile testing of HPT-processed pure Ta after 10 turns led to failure before the onset of plastic deformation [44] whereas tensile testing of HPT-processed pure Cu after 10 HPT turns gave elongations of ~4% [45]. This shows that the HPT-processed immiscible Cu-Ta alloy has a significantly improved elongation compared with either HPT-processed pure Ta or pure Cu. The reason for this reasonable elongation in the HPT-processed immiscible Cu-Ta alloy is probably related to the interfaces between the Cu-rich layers and the sparsely distributed Ta-rich flakes in the Cu-rich matrix, since this will affect the load transmission and initiation of dislocations between the interfaces and thereby permit an increased strain hardening capability and larger elongations.

5. Summary and conclusions

1. Nanostructured Cu-Ta alloys were successfully fabricated from Cu/Ta/Cu stacked discs by HPT processing at room temperature. A uniform two-phase layered microstructure was developed by increasing the numbers of HPT turns where these two phases included a Cu-rich layer with a composition of about $Cu_{81}Ta_{19}$ and a Ta-rich layer with a composition of about $Ta_{78}Cu_{22}$.

2.   Significant microstructural refinement was achieved in the Cu-Ta alloy with average crystallite sizes in the range of ~35-45 nm after 150 turns of HPT processing. In addition to Cu-Ta layers, there were also Ta-rich clusters on a fine-scale of <10 nm almost uniformly embedded within the matrix.

3.   After 150 turns of HPT processing, the Cu-Ta alloy exhibited remarkably improved hardness and tensile strength by comparison with commercial purity Cu and pure Ta. The average Vickers microhardness value was ~350 Hv, equivalent to ~3.43 GPa, and in tensile testing the UTS was ~1300 MPa with an elongation of about 40%.

4.   The results demonstrate the potential for using HPT processing at room temperature to create advanced microstructures and excellent mechanical properties that are not achieved through other processing routes.

Acknowledgements

Data Availability

The raw/processed data required to reproduce these findings cannot be shared at this time as the data also forms part of an ongoing study.

References

[1] R.Z. Valiev, A.P. Zhilyaev, T.G. Langdon, Bulk Nanostructured Materials: Fundamentals and Applications, Wiley/TMS, Hoboken, NJ, USA, 2014.

[2] K.A. Darling, M. Rajagopalan, M. Komarasamy, M.A. Bhatia, B.C. Hornbuckle, R.S. Mishra, K.N. Solanki, Extreme creep resistance in a microstructurally stable nanocrystalline alloy, Nature 537 (2016) 378-381.

[3] F. Abdeljawad, P. Lu, N. Argibay, B.G. Clark, B.L. Boyce, S.M. Foiles, Grain boundary segregation in immiscible nanocrystalline alloys, Acta Mater. 126 (2017) 528-539.

[4] T.B. Massalski (Ed.), Binary Alloy Phase Diagrams, ASM, Materials Park, OH, 1986.

[5] S. Zheng, J.S. Carpenter, R.J. McCabe, I.J. Beyerlein, N.A. Mara, Engineering interface structures and thermal stabilities via SPD processing in bulk nanostructured metals, Scientific Reports, 4 (2014) 4226(1-6).

[6] J.K. Han, J.D. Liss, T.G. Langdon, M. Kawasaki, Synthesis of a bulk nanostructured metastable Al alloy with extreme supersaturation of Mg, Scientific Reports, 9 (2019) 17186(1-7).

[7] J.K. Han, T. Herndon, J.I. Jang, T.G. Langdon, M. Kawasaki, Review: Synthesis of hybrid nanocrystalline alloys by mechanical bonding through high-pressure torsion, Adv. Eng. Mater. (in press) DOI: 10.1002/adem.201901289.

[8] R.Z. Valiev, T.G. Langdon, Principles of equal-channel angular pressing as a processing tool for grain refinement, Prog. Mater. Sci., 51 (2006) 881-981.

[9] H. Shahmir, T. Mousavi, J. He, Z. Lu, M. Kawasaki, T.G. Langdon, Microstructure and properties of a CoCrFeNiMn high-entropy alloy processed by equal-channel angular pressing, Mater. Sci. Eng. A 705 (2017) 411-419.

[10] L.F. Zeng, R. Gao, Q.F. Fang, X.P. Wang, Z.M. Xie, S. Miao, T. Hao, T. Zhang, High strength and thermal stability of bulk Cu/Ta nanolamellar multilayers fabricated by cross accumulative roll bonding, Acta Mater. 110 (2016) 341-351.

[11] A.P. Zhilyaev, G.V. Nurislamova, B.K. Kim, M.D. Baró, J.A. Szpunar , T.G. Langdon, Experimental parameters influencing grain refinement and microstructural evolution during high-pressure torsion, Acta Mater. 51 (2003) 753-765.

[12] A.P. Zhilyaev, T.G. Langdon, Using high-pressure torsion for metal processing: Fundamentals and applications, Prog. Mater. Sci. 53 (2008) 893-979.

[13] Y. Huang, P. Bazarnik, D. Wan, D. Luo, P. Pereira, M. Lewandowska, J. Yao, B. E. Hayden, T. G. Langdon, The fabrication of graphene-reinforced Al-based nanocomposites using high-pressure torsion, Acta Mater. 164 (2019) 499-511.

[14] Y. Huang, R.B. Figueiredo, T. Baudin, F. Brisset, T.G. Langdon, Evolution of strength and homogeneity in a magnesium AZ31 alloy processed by high-pressure torsion at different temperatures, Adv. Eng. Mater. 14 (2012) 1018-1026.

[15] R. Kulagin, Y. Beygelzimer, Y. Ivanisenko, A. Mazilkin, H. Hahn, High pressure torsion: from laminar flow to turbulence, IOP Conf. Series: Mater. Sci. Eng. 194 (2017) 012045(1-6).

[16] R. Kulagin, Y. Beygelzimer, Y. Ivanisenko, A. Mazilkin, B. Straumal, H. Hahn, Instabilities of interfaces between dissimilar metals induced by high pressure torsion, Mater. Lett. 222 (2018) 172-175.

[17] M. Pouryazdan, B.J.P. Kaus, A. Rack, A. Ershov, H. Hahn, Mixing instabilities during shearing of metals, Nature Commun. 8 (2017) 1611(1-7).

[18] P.H.R. Pereira, R.B. Figueiredo, Finite element modelling of high-pressure torsion: An overview, Mater. Trans. 60 (2019) 1139-1150.

[19] Y. Cao, Y.B. Wang, S.N. Alhajeri, X.Z. Liao, W.L. Zheng, S.P. Ringer, T.G. Langdon, Y.T. Zhu, A visualization of shear strain in processing by high-pressure torsion, J. Mater. Sci. 45 (2010) 765-770.

[20] Y. Cao, M. Kawasaki, Y.B. Wang, S.N. Alhajeri, X.Z. Liao, W.L. Zheng, S.P. Ringer, Y.T. Zhu, T.G. Langdon, Unusual macroscopic shearing patterns observed in metals processed by high-pressure torsion, J. Mater. Sci. 45 (2010) 4545-4553.

[21] Y. Cao, Y.B. Wang, R.B. Figueiredo, L. Chang, X.Z. Liao, M. Kawasaki, W.L. Zheng, S.P. Ringer, T.G. Langdon, Y.T. Zhu, Three-dimensional shear-strain patterns induced by high-pressure torsion and their impact on hardness evolution, Acta Mater. 59 (2011) 3903-3914.

[22] Y. Huang, M. Kawasaki, T.G. Langdon, Influence of anvil alignment on shearing patterns in high-pressure torsion, Adv. Eng. Mater. 15 (2013) 747-655.

[23] Y. Huang, M. Kawasaki, T.G. Langdon, An investigation of flow pattern and hardness distribution using different anvil alignments in high-pressure torsion, J. Mater. Sci. 48

(2013) 4533-4542.

[24] W. Jiang, X.H. An, S.D. Wu, Z.F. Zhang, R.B. Figueiredo, N. Gao, T.G. Langdon, Y. Zhu, On the heterogeneity of local shear strain induced by high-pressure torsion, Adv. Eng. Mater. 22 (2020) 1900477(1-8).

[25] Y.Z. Tian, X.H. An, S.D. Wu, Z.F. Zhang, R.B. Figueiredo, N. Gao, T.G. Langdon, Direct observations of microstructural evolution in a two-phase Cu-Ag alloy processed by high-pressure torsion, Scripta Mater. 63 (2010) 65-68.

[26] R. Kulagin, Y. Beygelzimer, A. Bachmaier, R. Pippan, Y. Estrin, Benefits of pattern formation by severe plastic deformation, Appl. Mater. Today 15 (2019) 236-241.

[27] A. Bachmaier, G.B. Rathmayr , M. Bartosik , D. Apel , Z. Zhang , R. Pippan, New insights on the formation of supersaturated solid solutions in CuCr system deformed by high-pressure torsion, Acta Mater. 69 (2014) 301-313.

[28] S. Sabooni, T. Mousavi, F. Karimzadeh, Fabrication and characterization of nanostructured Cu-15wt% Mo compound by mechanical alloying, International Journal of Modern Physics 5 (2012) 456-463.

[29] K.A. Darling, E.L. Huskins, B.E. Schuster, Q. Wei, L.J. Kecskes, Mechanical properties of a high strength Cu–Ta composite at elevated temperature, Mater. Sci. Eng. A 638 (2015) 322-328.

[30] S. Sabooni, T. Mousavi, F. Karimzadeh, Thermodynamic analysis and characterization of nanostructured Cu(Mo) compounds prepared by mechanical alloying and subsequent sintering, Powder Metallurgy 55(3) (2012) 222-227.

[31] N. Ibrahim, M. Peterlechner, F. Emeis, M. Wegner, S.V. Divinski, G. Wilde, Mechanical alloying via high-pressure torsion of the immiscible $Cu_{50}Ta_{50}$ system, Mater. Sci. Eng. A 685 (2017) 19-30.

[32] R.B. Figueiredo, P.H.R. Pereira, M.T.P. Aguilar, P.R. Cetlin, T.G. Langdon, Using finite element modeling to examine the temperature distribution in quasi-constrained high-pressure torsion, Acta Mater. 60 (2012) 3190-3198.

[33] A. Loucif, R.B. Figueiredo, M. Kawasaki, T. Baudin, F. Brisset, R. Chemam, T.G. Langdon, Effect of aging on microstructural development in an Al–Mg–Si alloy processed by high-pressure torsion, J. Mater. Sci. 47 (2012) 7815-7820.

[34] C. Suryanarayana, M.G. Norton, X-ray Diffraction: A Practical Approach, Plenum Press, New York, 1998, pp. 207.

[35] L. Lutterotti, S. Matthiers, H.R. Wenk, MAUD (Material Analysis Using Diffraction): A user friendly Java program for Rietveld texture analysis and more, Proceedings of the 12th international conference on textures of materials (ICOTOM-12), pp. 1599-1604, NRC Research Press, Ottawa, Canada, 1999.

[36] A. Denton, N. W. Ashcroft, Vegard's law, Phys. Rev. A 43 (1991) 3161-3164.

[37] B.D. Cullity, Elements of X-ray Diffraction, New York, 1956.

[38] J. Wongsa-Ngam, M. Kawasaki, T.G. Langdon, Achieving homogeneity in a Cu-Zr alloy processed by high-pressure torsion, J. Mater. Sci. 47 (2012) 7782-7788.

[39] S. Sabbaghianrad, M. Kawasaki, T.G. Langdon, Microstructural evolution and the mechanical properties of an aluminum alloy processed by high-pressure torsion, J. Mater. Sci. 47 (2012) 7789-7795.

[40] Materials Data Handbook, Cambridge University Engineering Department, Cambridge, UK, 2003.

[41] R.K. Koju, K.A. Darling, K.N. Solanki, Y. Mishin, Atomistic modeling of capillary-driven grain boundary motion in Cu-Ta alloys, Acta Mater. 148 (2018) 311-319.

[42] J. Chen, L. Lu, K. Lu, Hardness and strain rate sensitivity of nanocrystalline Cu, Scripta Mater. 54 (2006) 1913-1918.

[43] W. Qin, L. Fu, T. Xie, J. Zhu, W. Yang, D. Li, L. Zhou, Abnormal hardness behavior of Cu-Ta films prepared by magnetron sputtering, J. Alloys Compds. 708 (2017) 1033-1037.

[44] N. Maury, N.X. Zhang, Y. Huang, A.P. Zhilyaev, T.G. Langdon, A Critical examination of pure tantalum processed by high-pressure torsion, Mater. Sci. Eng. A 638 (2015) 174-182.

[45] M.Y. Alawadhi, S. Sabbaghianrad, Y. Huang, T.G. Langdon, Direct influence of recovery behaviour on mechanical properties in oxygen-free copper processed using different SPD techniques: HPT and ECAP, J. Mater, Res, Technol. 6(4) (2017) 369-377.
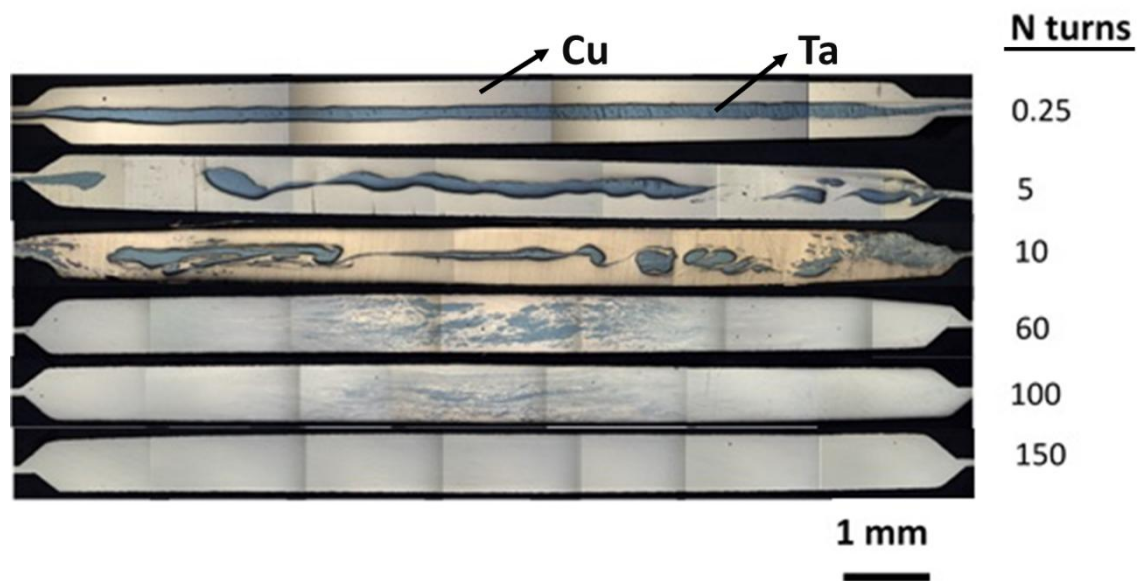
Figures captions

Fig. 1   Cross-sectional OM images of Cu/Ta/Cu stacks after different numbers of HPT turns: the dark regions are Ta and the bright regions are Cu.
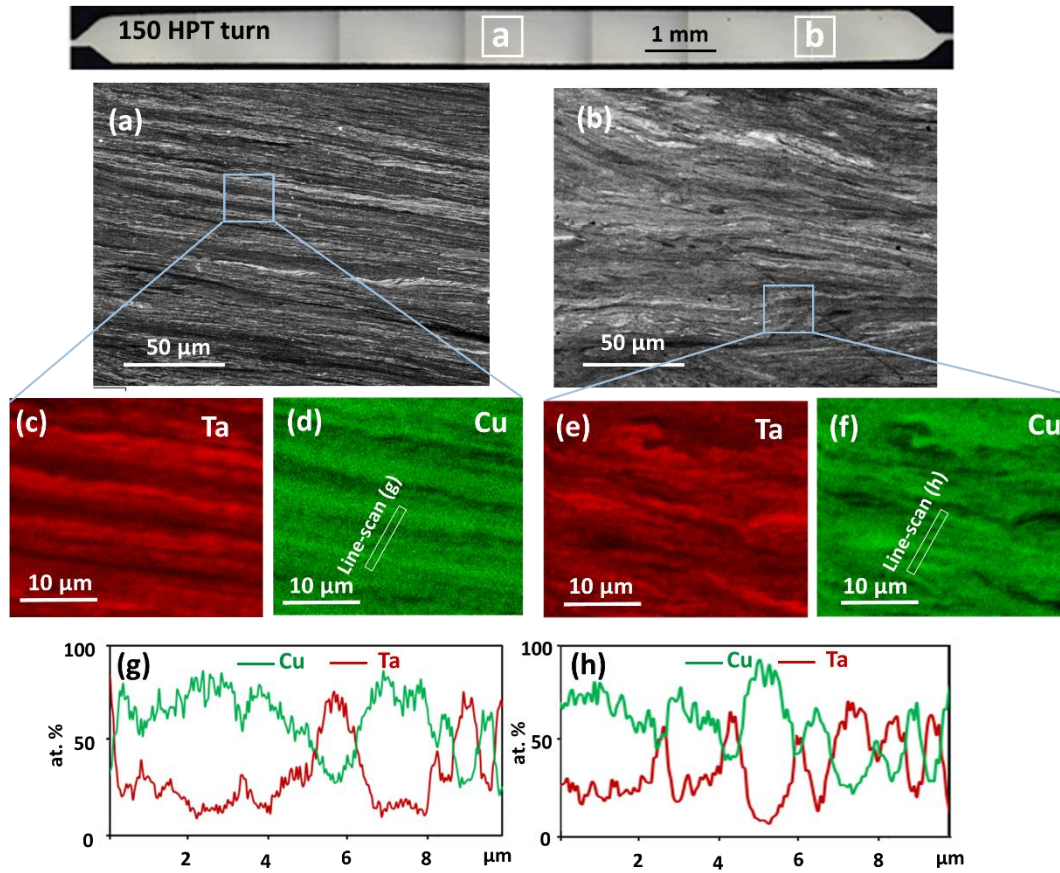
Fig. 2   Cross-sectional SEM images of the 150 turns sample at the areas marked (a) in the centre and (b) near the edge area, (c-f) elemental Cu and Ta maps of the indicated regions at higher magnifications, (g,h) EDX line scans over the region marked in d and f.
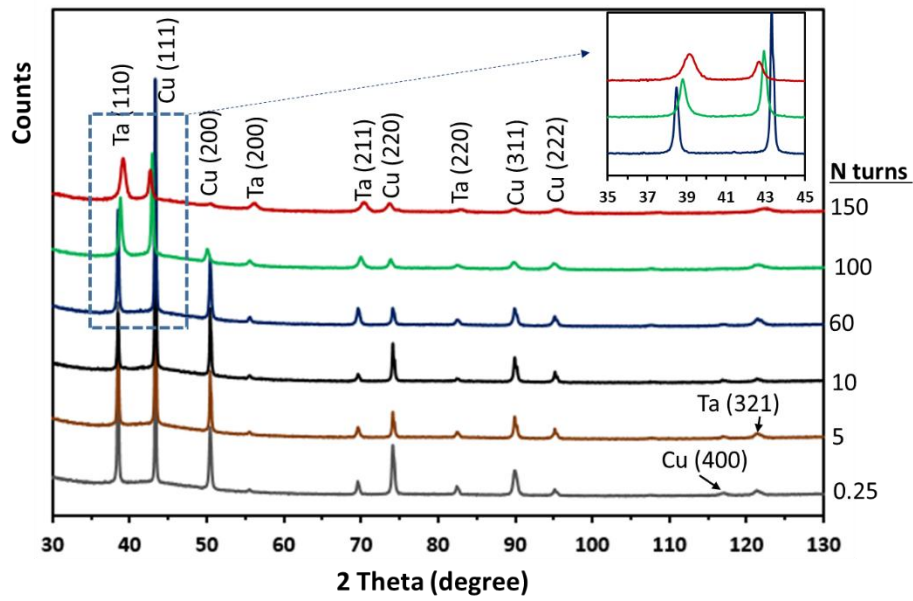
Fig. 3   The XRD patterns of the Cu-Ta discs processed by HPT at different numbers of turns (0.25, 5, 10, 60, 100 and 150). The inset shows the peak shifts for the Cu (111) and Ta (110) peaks after 100 turns.
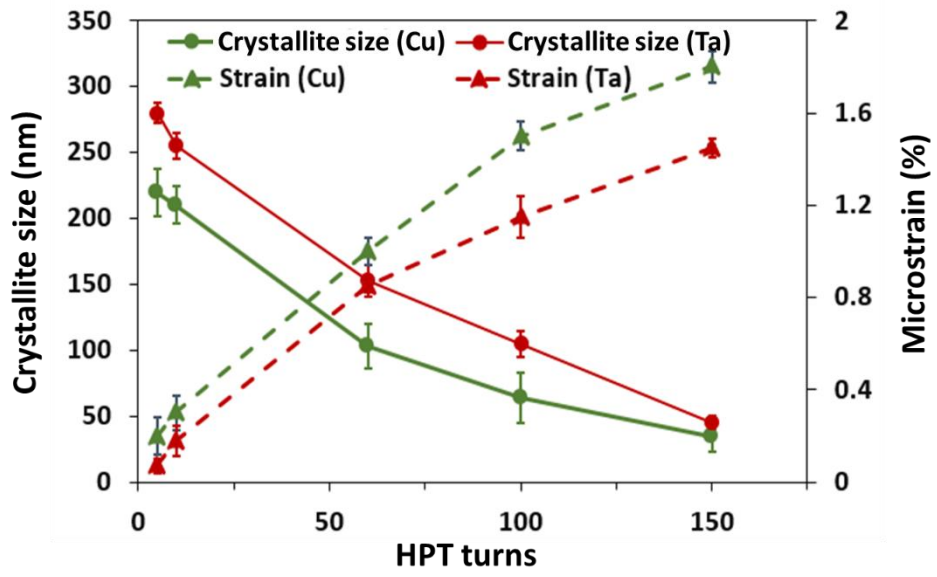
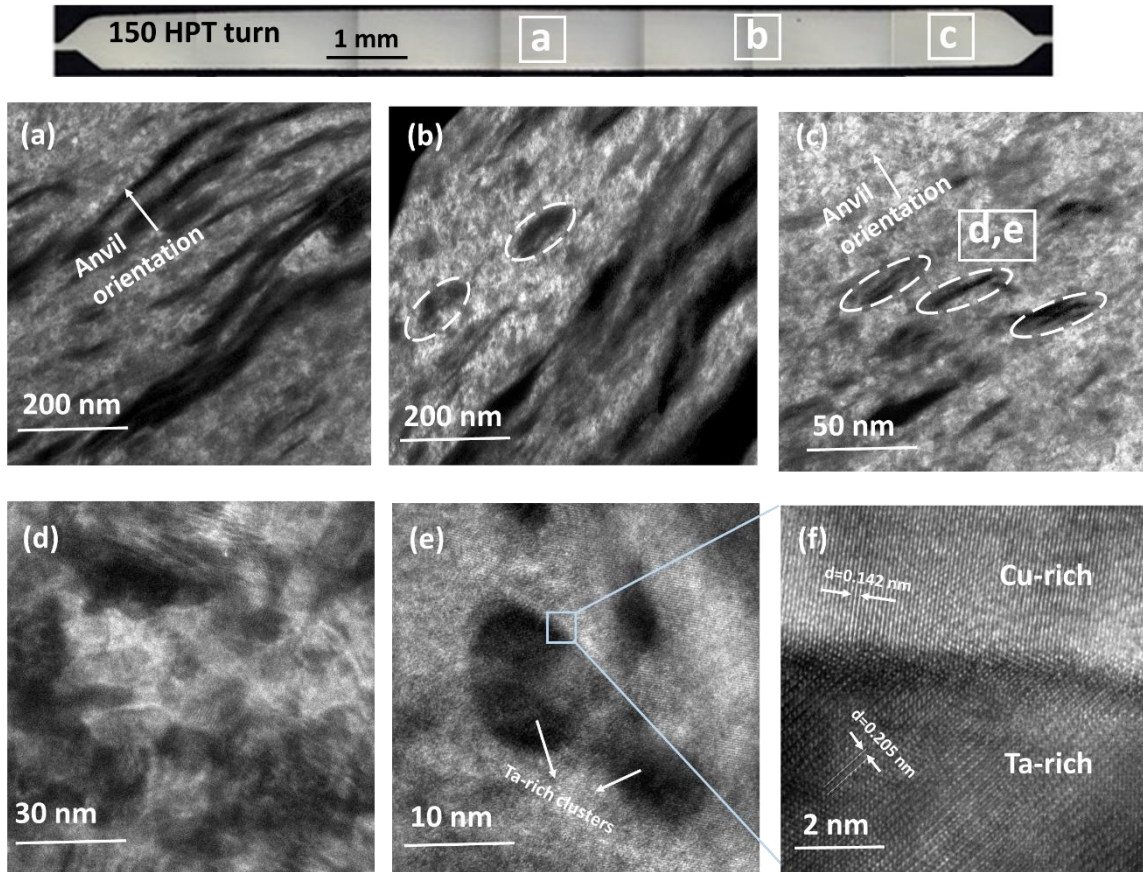Fig. 4   Crystallite size and lattice strain in Cu and Ta at various HPT turns.

Fig. 5   (a-c) TEM images of the Cu-Ta bulk after 150 HPT turns at different positions through the disc as indicated, (d,e) high magnification image of the matrix at the edge area and (f) atomic resolution TEM image of the interface between a Ta-rich region and the Cu-rich matrix.

Fig. 6   (a) STEM and (b) Z-contrast HAADF images of Cu-Ta sample after 150 HPT turns

Fig. 7   Colour-coded microhardness maps of the Cu/Ta/Cu stacks after different numbers of HPT turns

Fig. 8.   Stress-strain curve for the Cu-Ta bulk sample after processing through 150 HPT turns

Fig. 9   Schematic image illustrating the mechanism of microstructural evolution in the Cu-Ta bulk through HPT processing.

Figure

Fig. 1　Cross-sectional OM images of Cu/Ta/Cu stacks after different numbers of HPT turns: the dark regions are Ta and the bright regions are Cu.

Fig. 2 Cross-sectional SEM images of the 150 turns sample at the areas marked (a) in the centre and (b) near the edge area, (c-f) elemental Cu and Ta maps of the indicated regions at higher magnifications, (g,h) EDX line scans over the region marked in d and f.

Fig. 3 The XRD patterns of the Cu-Ta discs processed by HPT at different numbers of turns (0.25, 5, 10, 60, 100 and 150). The inset shows the peak shifts for the Cu (111) and Ta (110) peaks after 100 turns.

Fig. 4 Crystallite size and lattice strain in Cu and Ta at various HPT turns.

Fig. 5 (a-c) TEM images of the Cu-Ta bulk after 150 HPT turns at different positions through the disc as indicated, (d,e) high magnification image of the matrix at the edge area and (f) atomic resolution TEM image of the interface between a Ta-rich area and the Cu-rich matrix.

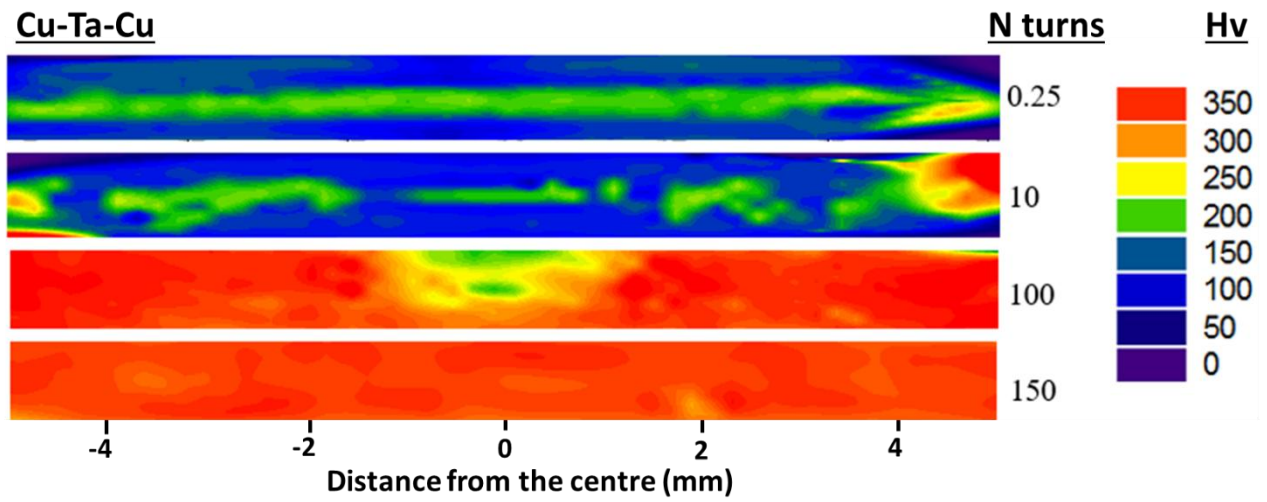Fig. 6 (a) STEM and (b) Z-contrast HAADF images of Cu-Ta sample after 150 HPT turns.

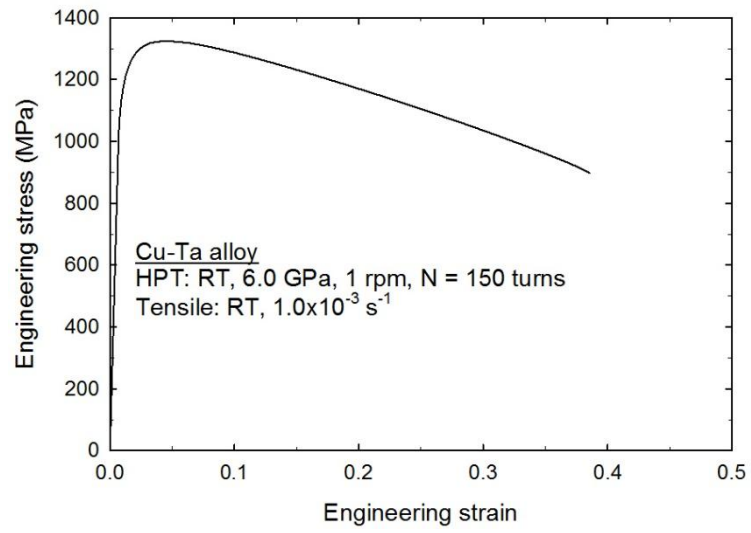Fig. 7 Colour-coded microhardness maps of the Cu/Ta/Cu stacks after different numbers of HPT turns.

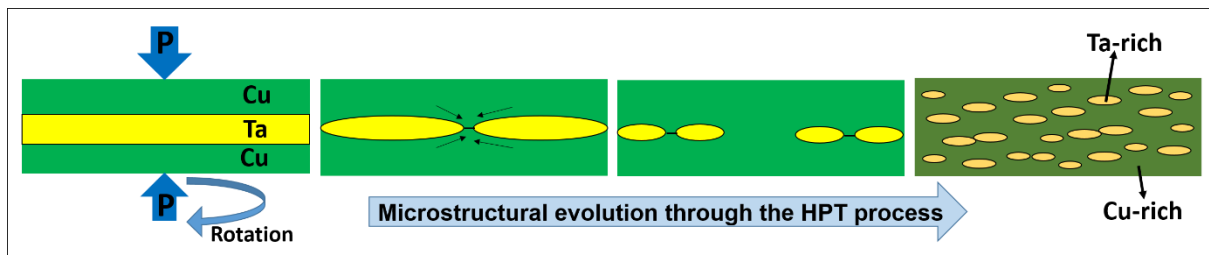Fig. 8. Stress-strain curve for the Cu-Ta bulk sample after processing through 150 HPT turns.

Fig. 9 Schematic image illustrating the mechanism of microstructural evolution in the Cu-Ta bulk through HPT processing.